Tetrahedron 70 (2014) 8023–8032

Contents lists available at ScienceDirect

Tetrahedron

journal homepage: www.elsevier.com/locate/tet

Ionic liquid-supported chiral saldach with tunable hydrogen bonding: synthesis, metalation with Fe(III) and in vitro antimicrobial susceptibility

Reda F.M. Elshaarawy [a,b,*], Christoph Janiak [b]

[a] Faculty of Science, Suez University, Suez, Egypt
[b] Institut für Anorganische Chemie und Strukturchemie, Heinrich-Heine Universität Düsseldorf, 40204 Düsseldorf, Germany

ARTICLE INFO

Article history:
Received 12 June 2014
Received in revised form 1 August 2014
Accepted 18 August 2014
Available online 23 August 2014

Keywords:
Imidazolium ionic liquids
Saldach
Mononuclear Fe(III) complexes
Antibacterial
Antifungal

ABSTRACT

New water-soluble methylimidazolium ionic liquids (MIILs) bearing *N,N′*-bis-(salicylidene)-*R,R*-1,2-diaminocyclohexane (saldach) scaffold, $H_2(R^1)_2$saldach(2-MeIm$^+$X$^-$)$_2$ (**4**a: R^1=H, X=Cl$^-$; **4**b: R^1=H, X=PF_6^-; **4**c: R^1=H, X=BF_4^-; **4**d: R^1=^{i}Pr, X=Cl$^-$; **4**e: R^1=^{i}Pr, X=PF_6^-; **4**f: R^1=^{i}Pr, X=BF_4^-), and their Fe(III) complexes have been synthesized and structurally characterized as well as their profile of antimicrobial susceptibility was identified. The new saldach-supported MIILs demonstrated a distinctly enhanced biocidal effect toward methicillin resistant *Staphylococcus aureus* (MRSA) and multidrug-resistant *Escherichia coli* (MDREC). Compound **4**d is the most potent antibacterial agent and could inhibit the growth of all micro-organisms, except *A. flavus*, more effectively than standard antibiotics.

1. Introduction

One of the most chemotherapeutic problems we are facing today in the context of fighting microbial infections is the relentless increase and spread of multidrug-resistant (MDR).[1,2] Thus, studies for the identification of novel targets and drugs for the treatment of infectious diseases are crucial. Several approaches to negate antibiotic resistance are currently being investigated, including inactivation of enzymes in essential metabolic pathways and inhibiting signal transduction systems.[3,4] These approaches involve the development of new antimicrobial drugs with modes of action that circumvent current resistance mechanisms.[5,6]

Interestingly, the saldach type compounds derived from salicylaldehyde and diamines exhibit versatile, steric, electronic, and liphophilic properties.[7] They are among the most relevant synthetic salen ligands with great potential applications in the synthesis of antibiotics, antiallergic, antiphlogistic, and antitumor drugs.[8,9] Growing attention has been devoted to these materials due to their low cost, ease of fabrication, and their stability.[10] A prototropic tautomeric attitude has been recognized in a number of *o*-hydroxy Schiff bases,[11] which is of interest mainly due to the existence of O–H···N and N–H···O type hydrogen bonds in enol-imine and keto-enamine tautomers, respectively.[12] These H-bonding interactions play a key role in preferential solvation and have been investigated as sources of variety of potential chemical, biochemical, and pharmacological events. Metallosaldach compounds have become a subject worthy of pursuit and have demonstrated great promise for their extensive applications in catalysis as chemical nucleases that bind, cleave, and damage nucleic acids[13,14] via oxidative alkylation of nucleobases.[15] Furthermore, various Fe(III)-saldach derivatives have been implicated in efficient asymmetric catalysis and in catalyzing the hydrolytic cleavage of DNA and RNA.[16]

In the race to synthesize new pharmaceutical drugs, dialkylimidazolium ionic liquids have become attractive candidates for application in medicinal chemistry due to their tunable properties and ability to generate biological responses upon binding to several biological targets. They have been recognized as bactericidal,[17] fungicidal,[17] acetylcholinesterase (AChE) inhibitor,[18] for delivery of anti-inflammatory drugs,[19] local anesthetic,[17] anti-nociceptive, anticholinergic, and anticancer drugs.[20] Carson et al. have reported the broad spectrum antibiofilm activity of 1-alkyl-3-methylimidazolium chloride ILs against a panel of clinically important microbes.[21]

* Corresponding author. Tel.: +20 1228123965; e-mail addresses: Reda.El-Shaarawy@uni-duesseldorf.de, reda_elshaarawi@science.suez.edu.eg, reda_shaarauy@yahoo.com (R.F.M. Elshaarawy), janiak@uni-duesseldorf.de (C. Janiak).

http://dx.doi.org/10.1016/j.tet.2014.08.034
0040-4020/

Despite extensive work done on salen ligands, little attention has been paid to the saldach Schiff bases.[22,23] To the best of our knowledge, there are very few reports about the fabrication of ionic liquids-supported saldach-Schiff bases.[24]

condensation. These ligands were isolated in high yields and structurally characterized by elemental analysis and spectral methods, FTIR, UV–Vis, NMR (^{1}H, ^{13}C, ^{19}F, ^{31}P), MS (ESI, MALDI-TOF), as well as conductivity measurements.

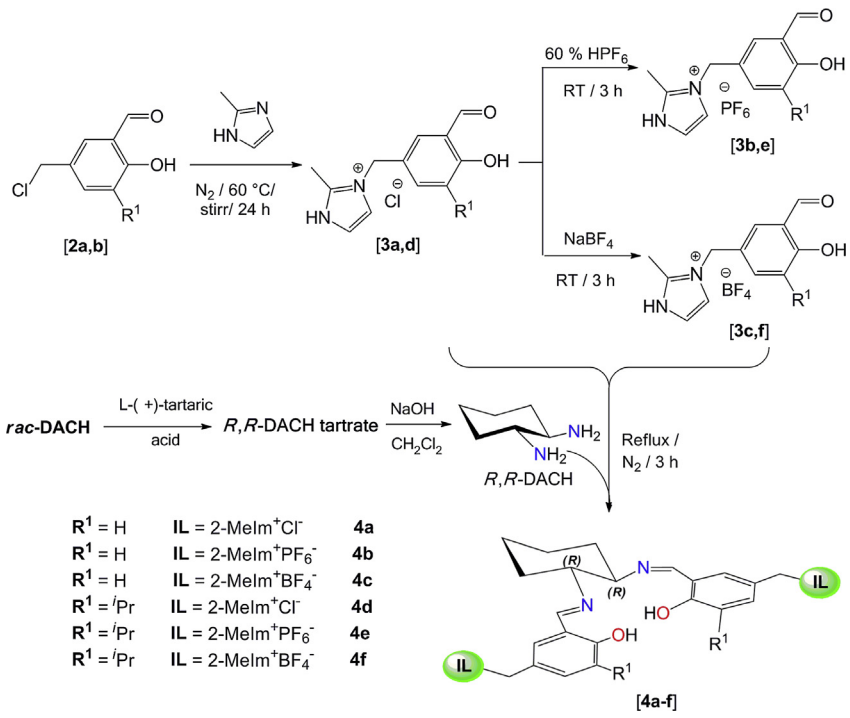

Scheme 1. Synthesis of salicylaldehyde-imidazolium salts (**3a**–**f**) and saldach-imidazolium architectures (**4a**–**f**).

In continuation of our ongoing programs directed toward the development of novel materials[25] for potent, selective, and less toxic therapeutic agents,[26] we now report a concise, practical synthetic route and in vitro antimicrobial assessment of novel saldach-bis-(imidazolium) salts and their Fe(III) complexes, which may allow us to develop a new promising therapeutic strategy to combat antibiotic resistance.

2. Results and discussion

2.1. Chemistry

2.1.1. Synthesis of chiral R,R-(H_2(R)$_2$saldach(MeIm$^+X^-$)$_2$). The synthesis of saldach-scaffold bearing imidazolium ionic liquid (IL) terminals (**4a**–**f**) is depicted in Scheme 1. The key starting materials salicylaldehydes-imidazolium salts (**3**a–f) were synthesized starting from salicylaldehyde derivatives (**1a,b**) following modified literature procedures.[27] Under HCl_g atmosphere, salicylaldehydes (**1a,b**) were chloromethylated with $(CH_2O)_n$/HCl_{aq} in the presence of a catalytic amount of $ZnCl_2$ to give 5-chloromethyl-salicylaldehydes (**2**a,b) in high purity, which are used as an alkylating agent for the quaternization of 2-methylmidazole to generate the common precursors salicylaldehydes-imidazolium chlorides (**3a,d**). Anion metathesis of these precursors with hexafluorophosphoric acid ($HPF_{6(aq)}$) and sodium tetrafluoroborate yield the corresponding hexafluorophosphate salt (**3b,e**) and tetrafluoroborate salt (**3c,f**), respectively. Eventually, the desired IL–saldach ligands, *R,R*-(H_2(R)$_2$saldach(MeIm$^+X^-$)$_2$) (**4a**–**f**), were synthesized by the salicylaldehydes-imidazolium salts (**3a**–**f**)/*R,R*-dach Schiff-base

2.1.2. Synthesis of Fe(III)saldach-imidazolium salts, [Fe(III)Cl {(R)$_2$saldach(MeIm$^+X^-$)$_2$}]. The iron(III) complexes, [Fe(III)Cl {(R)$_2$saldach(MeIm$^+X^-$)$_2$}] (**6**a–f), were easily prepared by refluxing a solution of the corresponding saldach ligands with anhydrous iron(III) chloride in methanol (UV-spectroscopy grade) under aerobic conditions (Scheme 2).

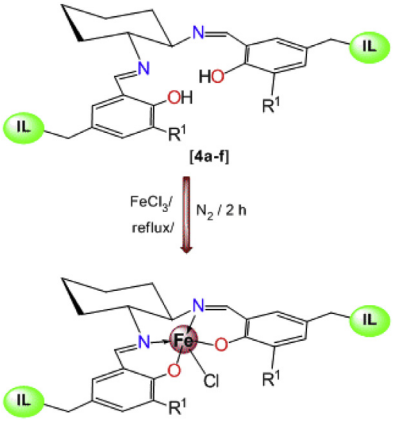

Scheme 2. Metalation of Fe(III) ion to saldach-imidazolium salts.

Unfortunately all attempts to obtain X-ray diffraction quality single crystals of the free ligands and their Fe(III) complexes using different crystallization techniques (such as slow evaporation, over-layering, liquid–liquid diffusion, and differential

cooling) were unsuccessful. Yet, the structures of metal–ligand complexes in this work were proposed based upon elemental and spectral analysis (FTIR, UV–Vis, MALDI-TOF) as well as conductivity measurements and matching with the structures of previously reported metal-saldach analogues (Table S1, supplementary data).

2.2. Characterizations of the saldach-bis(imidazolium) salts and their complexes

2.2.1. Microanalytical data and conductivity. Saldach-bis(imidazolium) salts (**4a**–**f**) and their complexes (**5a**–**f**) were prepared in high yields, gave satisfactory C, H, and N elemental analyses, which are consistent with the proposed formula for the ligands and their chelates (see the Experimental section).

Molar conductance values of all the chiral *R*,*R*-saldach-bis-(imidazolium) salts and their complexes in EtOH (1×10^{-3} M) at 25 °C are in the region of 71.5–349.0 μS/cm in accordance with their ionic nature.

2.2.2. IR spectroscopic data. Infrared spectroscopy confirmed the anchoring of the central saldach backbone to the terminal imidazolium groups, the presence of $H_2(R^1)_2$saldach$(IL)_2$ ligands as well as their binding mode to the iron(III) center, within the complexes. The selected IR spectra of the novel Schiff bases, *R*,*R*-$H_2(R^1)_2$saldach$(IL)_2$, and their iron(III) complexes along with their tentative assignments are reported in Table 1. There are three main peaks (C=N stretching vibrations: 2291–2313; X^- vibrations: 570–591 cm^{-1}, for Cl^-, 837–841 cm^{-1}, for PF_6^-, and 1059–1061 cm^{-1}, for BF_4^-; Im bending vibrations: 758–765 cm^{-1}), which are related to the imidazolium ionic liquid terminals. Noteworthy, the broad peaks, which appeared in the range of 3000–3100 cm^{-1} can be assigned as peaks associated with the interaction of aromatic C–H with X^-.[28]

Table 1
Assignment of the vibrations[a] from saldach-bis-(imdazolium) salts (**4a**–**f**) and their Fe(III) complexes (**5a**–**f**)

Compd.	$\nu_{(O-H)}$	$\nu_{(C=N)}$	$\Delta\nu_{(C=N)}$	$\nu_{(Ph-O)}$	$\Delta\nu_{(Ph-O)}$	$\nu_{(Fe-N)}$	$\nu_{(Fe-O)}$
4a	3345	1630	—	1274	—	—	—
5a	3441	1617	−13	1281	+7	547	471
4b	3329	1637	—	1276	—	—	—
5b	3516	1620	−17	1283	+7	542	468
4c	3323	1636	—	1273	—	—	—
5c	3498	1619	−17	1282	+9	539	467
4d	3334	1629	—	1271	—	—	—
5d	3498	1613	−14	1282	+11	545	467
4e	3332	1633	—	1273	—	—	—
5e	3430	1617	−16	1287	+14	557	471
4f	3339	1631	—	1274	—	—	—
5f	3442	1622	−9	1284	+10	550	465

[a] Assignments according to Refs. 27–30.

The three prominent bands at 3323–3345, 1629–1637, and 1270–1282 cm^{-1} are characteristic for the saldach structural motif. The broad stretch around 3334 cm^{-1}, is assigned to an intramolecular hydrogen bond involving the phenolic OH group, and a medium intensity band in the range of 1276±6 cm^{-1} is attributed to ν_{Ar-O}. Interestingly, the vibration at the region 1633±4 cm^{-1} may be assigned to the aldimine C=N stretch.[29,30] This indicates that the central saldach backbone is in the expected *O*-protonated, enol-imine, tautomeric form in the solid state (Scheme 3).

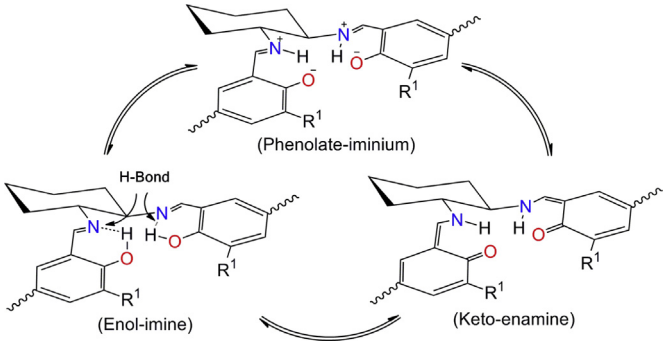

Scheme 3. Possible tautomeric forms and intra-molecular hydrogen-bonding in saldach backbone of $H_2(R^1)_2$saldach$(IL)_2$.

When comparing the spectroscopic data of Fe(III) complexes with those of the free ligands (see Fig. S1, supplementary data), marked changes may be noticed in the ligand bands arising from various modes of donor groups involved in bonding to iron ions. The broad phenolic–OH stretches in the FTIR spectra of the saldach starting materials at ca. 3330 cm^{-1} were missing from the spectra of the Fe(III) complexes indicating deprotonation of the phenolic oxygen and replacement of H by the ferric ion. This was further supported by the high-energy shift of the phenolic C–O stretching frequency by 7–14 cm^{-1} in the spectra of complexes. This is evidence for the ligation of the phenolate oxygen to Fe(III) ion, the growth of a new band around 465–471 cm^{-1}, which is assigned to the ν_{Fe-O} vibration provides an additional support. Also consistent with the complex formation and the participation of azomethine nitrogen in bonding[31] was the observation that the strong $\nu_{C=N(azomethine)}$ stretches in the FTIR spectra of the free ligands were displaced to lower frequency, by 9–17 cm^{-1}, in complexes (cf. Table 1). This is further confirmed by the appearance of a new band at 542–557 cm^{-1} assigned to a ν_{Fe-N} vibration.[32] Finally, the broad band at ca. 3440–3500 cm^{-1} agrees with the hydrated nature of complexes as suggested by the microanalytical data.

In conclusion, infrared spectroscopic data suggests that, *R*,*R*-$H_2(R^1)_2$saldach$(IL)_2$ compounds act as tetradentate N_2O_2-chelating ligands.

2.2.3. NMR studies and tautomerism scenario. The possible tautomeric equilibria with their relative tautomer, imine/enamine, population in saldach-bis-imdazolium salts **4a**–**f** can be assigned on the basis of NMR data. The enol-imine tautomer can easily be identified by the presence of two singlets in the 1H NMR spectra: one deshielded signal (~13–15 ppm) corresponding to the phenolic proton and the other attributed to the –CH=N imine proton (~8.5–9.5 ppm). On the other hand, a keto-enamine structure shows two coupled doublets: one for the NH proton, which is significantly deshielded (~14–16 ppm), and one for the enamine =CH–N– proton (~8.5–10 ppm). Noteworthy, the multiplicity of such signals is the key to distinguish them as chemical shifts are quite similar in both tautomers.[33] Table 2 contains some relevant NMR data for compounds **4a**–**f**. There are common spectral peculiarities of the spectra ^{1}H NMR for the compounds H_2saldach$(MeIm^+X^-)_2$ (**4a**–**c**) represented in the two characteristic doublet signals around 13.97 ppm and 8.78 ppm, typical for an enamine group.

Clearly the multiplicity of such signals and the absence of singlets, corresponding to the phenolic proton, are the keys to suggest that, the saldach backbone, in **4a**–**c**, is not in the expected *O*-protonated tautomeric form but in the *N*-protonated tautomeric form. However, the C-1 signal in **4a**–**c**, which resonates at ~168 ppm,

Table 2
Selected (^{1}H/^{13}C) NMR spectroscopic data[a] for **4a**–**f**

Nr.	O**H**/N**H** ($J_{NH,H}$)	N–**CH** ($J_{CH,H}$)	H**C**···N	**C**-1	K_T	Imine (%)
4a	13.97 (s, 2H) (0.0)	8.82 (s, 2H) (0.0)	160.21	171.29	1.20	45.41
4b	14.02 (d, 2H) (2.35)	8.74 (d, 2H) (1.98)	161.93	172.00	1.38	41.95
4c	13.93 (d, 2H) (3.24)	8.77 (d, 2H) (2.01)	161.25	173.32	1.78	35.96
4d	13.87 (s, 2H) (0.0)	8.60 (s, 2H) (0.0)	160.01	165.24	0.33	74.93
4e	13.98 (s, 2H) (0.0)	8.53 (s, 2H) (0.0)	160.10	164.93	0.31	76.44
4f	14.04 (s, 2H) (0.0)	8.55 (s, 2H) (0.0)	159.79	165.13	0.32	75.46

[a] δ in ppm and J in Hz.

which is between the phenolic carbon, ~160 ppm for an enol-imine, and the carbonyl chemical shift, ~180 ppm for a pure keto-enamine tautomer,[34] together with small coupling constants ($J_{NH,H}$=2.35–3.24 Hz) is evidence again of a rapid imine-iminium-enamine equilibrium in DMSO-d_6 solution at room temperature (cf. Scheme 3).

On the other hand, the ^{1}H NMR spectral data of $H_2(^iPr)_2$saldach(MeIm$^+$X$^-$)$_2$ (**4d**–**f**) reflects a different signature. Two singlets at ca. 14 ppm, due to phenolic O–H, and around 8.56 ppm, due to iminic protons, are typical for an enolimine tautomer. This splitting pattern was proposed for the pure *O*-protonated tautomer, however, the C-1 resonated at ca. 165 ppm, which is intermediate between these of the aldimine and the ketimine values.[35] Thus, NMR studies demonstrate that, in **4**d–f the central saldach backbone is in the enolimine form with some contribution of the ketoenamine form in the solution (cf. Scheme 3).[36]

The competitive H-binding between the oxygen and nitrogen groups was assigned based on the tautomeric equilibrium constants (K_T), calculated from the ^{13}C shifts of the phenolic carbon.[37]

The experimentally observed ^{13}C chemical shifts (δ_{exp}) are an average of those of tautomeric, pure imine or iminium and pure enamine forms (δ_i and δ_e, respectively). Accordingly, $\delta_{exp}=n_i\delta_i+n_e\delta_e$, where n_i and n_e denote the molecular populations of imine and enamine tautomers, respectively (obviously, $n_i+n_e=1$). These simple equations can therefore be used to estimate tautomeric populations, assuming that δ_i/δ_e values are known. Thus:

$$n_i = (\delta_e - \delta_{exp})/(\delta_e - \delta_i) \text{ and } n_e = (\delta_{exp} - \delta_i)/(\delta_e - \delta_i)$$

The tautomeric constant (K_T=[enamine]/[imine]=n_e/n_i) for imine-enamine equilibria may then be expressed by:

$$K_T = n_e/n_i = (\delta_{exp} - \delta_i)/(\delta_e - \delta_{exp}) \quad (1)$$

These tautomerization constants can be calculated using representative δ_i (160.1 ppm) and δ_e (180.6 ppm) values for pure enol-imine and pure keto-enamine forms, respectively.[34] Consequently, Eq. 1 can be rewritten as:

$$K_T = n_e/n_i = (\delta_{exp} - 160.1)/(180.6 - \delta_{exp}) \quad (2)$$

The results obtained by application of Eq. 2 are collected in Table 2. These data demonstrate that, the steric effect of bulky *ortho*-substituent (isopropyl) to free phenolic hydroxyl group in saldach backbone decreases the rate of enol/keto interconversion.

2.2.4. Electronic absorption spectroscopy. UV–vis spectra of $H_2(R)_2$saldach(MeIm$^+$-X$^-$)$_2$ (**4a**–**f**) exhibit two strong absorptions, the first one centered at ca. 253 nm, for **4a**–**c**, or 259 nm, for **4d**–**f**, originate from the $\pi\rightarrow\pi^*$ and $n\rightarrow\pi^*$ transitions associated with the phenolic chromophor,[38] while the other peak around 320 nm can be assigned to the $\pi\rightarrow\pi^*$ transition involving the imine group[38] (see Table S2 in supplementary data).

By going from the free *R*,*R*-saldach-bis-(imdazolium) salts to their mononuclear Fe(III) complexes (**5**a–f), the UV–Vis spectra give further evidence for ligation. Electronic spectra of these complexes are similar and consist of three regions of absorption. The most important feature in the near-UV region, is the shift of the imine $\pi\rightarrow\pi^*$ transition from 319.5 nm and 325 nm in free ligands to higher wavelengths over 380 nm and 400 nm (see Fig. 1), which indicates coordination of a metal ion with ligands.[39] In addition, the low intensity broad absorption band above 500 nm can be assigned to the three allowed d–d transitions, ($d_{xz}\rightarrow d_{x2-y2}$), ($d_{xy}\rightarrow d_{x2-y2}$, d_{yz}), and ($d_{z2}\rightarrow d_{x2-y2}$),[40] assuming a square pyramidal geometry with the [FeN_2O_2Cl] chromophore.

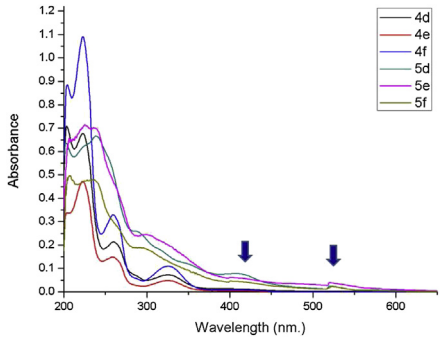

Fig. 1. UV–Vis Spectral Data (λ_{max} nm) for the saldach-imidazolium salts (**4d**–**f**) and their Fe(III)-complexes (**5d**–**f**).

3. Pharmacology

Many clinical trials of new active pharmaceutical ingredients (API) end in failure due to the low efficacy of the drug because of limited bioavailability or solubility. Anchoring of imidazolium ionic liquid terminals to the $H_2(R)_2$saldach could provide a synergetic effect of improving water solubility and at the same time enhancing the pharmacological effect.

3.1. Differential antibacterial efficacy

The target imidazolium IL-supported saldach ligand, their complexes, and standards drugs were in vitro assessed separately for their capacity to inhibit the growth of a range of clinically significant pathogenic bacterial strains including MRSA (methicillin resistant *Staphylococcus aureus*) and MDREC (multidrug-resistant *Escherichia coli*) (see ZOIs, Fig. 2).

In general, our data demonstrate that the incorporation imidazolium-anion pairs exerts an overall additive effect: (i) ameliorates the water-solubility of saldach/(saldach)Fe(III); (ii) leads to the formation of new architectures with an enhanced synergistic antimicrobial effects of the 2-methylimidazolium ionic liquids and saldach/(saldach)Fe(III) biochromophores, especially against Gram-positive bacteria. As shown in Fig. 2, the growth of MRSA, *B. subtilis*, and MDREC was inhibited by most of the target compounds at all tested concentrations and the ZOI varies in a dose-dependent profile while *P. aeruginosa* was resistant to most of these compounds at low concentrations, 0.25–5 mM. The lower MIC values (Table 3) of the screened compounds **4**,**5a**–**f** to G$^+$-bacterial strains (*S. aureus*, B. subtilis) are interesting when compared to G$^+$ ones (*S. aureus*, B. subtilis). For example, the MIC of **5d** to methicillin resistant (MR) *S. aureus*, 2.08 mM, was 6.5-fold lower compared to multidrug-resistant (MDR) *E. coli*, 13.87 mM. These results

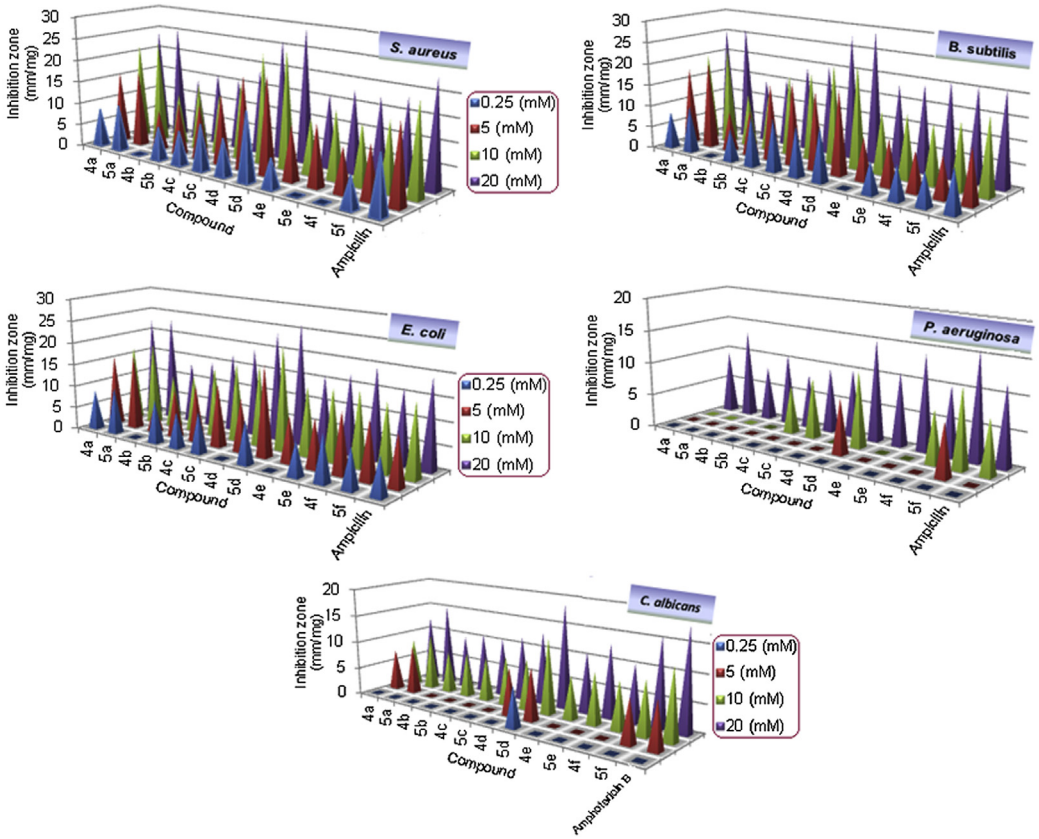

Fig. 2. Graph of zone of inhibition/mm for target compounds against different bacterial and fungal species.

Table 3
MIC (mM) profiles of the saldach-imidazolium salts and their Fe(III) complexes against different strains[a]

Nr.	MIC (mM)					
	S. aureus	*B. subtilis*	*E. coli*	*P. aeruginosa*	*A. flavus*	*C. albicans*
4a	16.09	16.99	18.12	>10,000	−ve	>250
5a	9.85	**9.55**	14.83	>5000	−ve	>250
4b	>250	>250	>250	>10,000	−ve	>5000
5b	25.13	21.97	29.89	>10,000	−ve	>5000
4c	21.23	19.85	23.48	>5000	−ve	>5000
5c	17.86	14.76	18.01	>5000	−ve	>5000
4d	10.21	12.14	>250	>5000	−ve	>250
5d	**2.08**	**3.29**	13.87	>250	−ve	**75.21**
4e	20.39	>250	>250	>10,000	−ve	>5000
5e	15.77	37.50	30.71	>10,000	−ve	>5000
4f	>250	26.53	15.63	>5000	−ve	>5000
5f	18.11	19.65	11.58	>250	−ve	>250
Am.	**12.50**	**20.00**	**15.00**	**>1000**	−ve	−ve
Am. B	−ve	−ve	−ve	−ve	**40.00**	**80.00**

The bold values refer to the MIC of the most potent compounds compared to these of standard drugs Am. and Am. B.
Am.=Ampicillin (Antibaterial drug).
Am. B=Amphotericin B (Antifungal drug).
[a] *S. aureus* and *B. subtilis*, representative for G^+ Bacteria, *E. coli*, and *P. aeruginosa*, as G^- Bacteria, while *A. flavus* and *C. albicans* for Fungi.

demonstrate the stronger biocidal action for gram-positive, compared with gram-negative bacteria.

The effectiveness of saldach-imiazolium/Fe(III)saldach-imiazolium salts in the destruction of Gram-positive bacteria may depend on two synergistic factors: (i) the saldach/Fe(III)saldach/imidazolium cell penetration effects and (ii) the intracellular imidazolium/Fe effects. As already confirmed in our previous study.[27] interaction between positively charged imidazolium terminals and the cell wall of bacteria could be facilitated by the relative abundance of negative charges on Gram-positive bacterial surface so that saldach-imidazolium/Fe(III)saldach-imidazolium could penetrate easily into the cell. Once these imidazolium-based architectures are translocated into the cell, they will strongly associate with the cellular components that caused the highest inhibition of bacterial growth. Compared to *S. aureus* and B. subtilis, the surfaces of E. coli are less negatively charged and more rigid,[41] therefore, their resistance to saldach-imidazolium/Fe(III)saldach-imidazolium salts is higher than *S. aureus* and B. subtilis. Notably, incorporation of Fe(III) ion improves the bactericidal efficacy of parent saldach-supported methylimidazolium ionic liquids (MIILs). The generation of reactive oxygen species (ROS)[42] that able to damage essential signal cascades in the pathogen or DNA interaction followed by induction of apoptosis would be a possible explanation for the mode of action, which is depended on the presence of an iron center.

To further understand the differential antibacterial effect of different imidazolium ILs-supported saldach species, the effect of structural variability of the saldach backbone and the imidazolium ends upon the bactericidal efficacy was studied in order to evaluate the structure−activity relationship (SAR). As shown in Table 4, the *R,R*-enantiomers (MIC=2.08−18.12 mM) were somewhat more active than its *rac*-configurated isomers (MIC=6.01−19.23 mM). Furthermore, the inhibitory effect of *R,R*-enantiomers on the microbes increases in the order of *P. aeruginosa*<*E. coli*<*B. subtilis*<*S. aureus*. Configurations at the asymmetric C-atoms of cyclohexane moiety determine its orientation relative to the iron plane. In the case of *R,R*-configurated compounds, a coplanarity of the most likely chair conformation and the chelate ring could be assumed, which could be considered as a reason for this enhanced *R,R*-saldach-DNA interactions in comparison to the *meso*-isomer. The 3D structure of the *R,R*-[Fe^{III}(saldach)Cl] core (see Fig. 3) allows a DNA

intercalation by the Fe(III)sadach chromophore while the cyclohexane ring, located perpendicular to the $[FeN_2O_2Cl]$ core, would hinder or even prevent the intercalation between nucleobases.

Table 4
Relationship between antimicrobial ability, MIC (mM), and substituent/configuration of saldach skeleton[a]

Compound	MIC (mM)				
	S. aureus	*B. subtilis*	*E. coli*	*P. aeruginosa*	*C. albicans*
R,R-Saldach (**4**a)	16.09	16.99	18.12	>10,000	>250
R,R-Fe^{III}saldach (**5**a)	9.85	**9.55**	14.83	>5000	>250
rac-Saldach	17.60	17.50	19.23	>10,000	>250
rac-Fe^{III}saldach	14.85	16.03	10.16	>10,000	>250
R,R-^{i}Pr-saldach (**4**d)	10.21	12.14	>250	>5000	>250
R,R-Fe^{III}Prsaldach (**5**d)	**2.08**	**3.29**	13.87	>250	**75.21**
rac-^{i}Pr-aldach	12.11	13.35	>250	>5000	>250
rac-Fe^{III}Prsaldach	8.73	6.01	14.76	>250	83.22
Ampicillin	**12.50**	**20.00**	**15.00**	**>1000**	−ve
Amphotericin B	−ve	−ve	−ve	−ve	**80.00**

The bold values refer to the MIC of the most potent compounds compared to these of standard drugs Am. and Am. B.
[a] *S. aureus* and *B. subtilis*, representative for G$^+$ Bacteria, *E. coli*, and *P. aeruginosa*, as G$^-$ Bacteria, while *C. albicans* for Fungi.

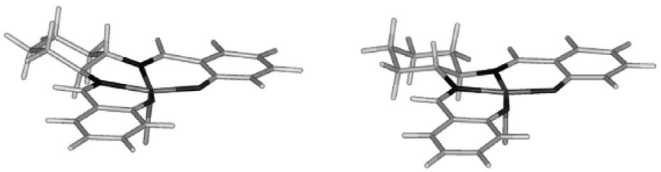

Fig. 3. Conformations of the *R,R*-[Fe^{III}(saldach)Cl] core.[40]

Note that, exchange of the hydrogen atom by an *iso*-propyl group results in a decrease of the MICs, indicative of the antibacterial effectiveness of saldach-MIILs being a consequence of the presence of the alkyl substituents at the saldach backbone. This might be attributed to the enhanced lipophilicity of ^{i}Pr-saldach, in **4**,**5d**–**f**, compared to H-saldach, in **4**,**5a**–**b**, which facilitates the cell-walls penetration by simply dissolving into and through the lipophilic cell wall and accumulate in mitochondria (relative to cytosol) to a much higher extent.

Saldach-bis-imidazolium chloride, hexafluorophosphate and tetrafluoroborate (**4a**–**f**) and their complexes (**5a**–**f**) showed different levels of bactericidal properties against the tested pathogens. The saldach-imidazolium chlorides (**4a**) (MIC=16.09$_{S.\ aureus}$, 16.99$_{B.\ subtilis}$, 18.12$_{E.\ coli}$ mM), (**4d**) (MIC=10.21$_{S.\ aureus}$, 12.14$_{B.\ subtilis}$ mM), and their Fe(III) chelates (**5**a) (MIC=9.85$_{S.\ aureus}$, 9.55$_{B.\ subtilis}$ mM), (**5d**) (MIC=2.08$_{S.\ aureus}$, 3.29$_{B.\ subtilis}$ mM) are the most effective in inhibition of bacterial growth. Chloride metathesis with PF_6 and BF_4 anions resulted in a decrease of bactericidal activities of imidazolium-supported saldach salts. For example, the counterion-dependent antibacterial activity of [Fe^{III}Cl(^{iso}Pr-saldach(MeIm$^+$X$^-$)$_2$)] against *S. aureus* and *E. coli* follows the trend below:

$$X\ (\text{MIC mM})_{S.aureus}: BF_4\ (18.11) < PF_6\ (15.77) < Cl\ (2.08)$$
$$X\ (\text{MIC mM})_{B.subtilis}: PF_6\ (37.50) < BF_4\ (19.65) < Cl\ (3.29)$$
$$X\ (\text{MIC mM})_{E.coli}: PF_6\ (30.71) < Cl\ (13.87) < BF_4\ (11.58)$$

Lipophilicity and/or vulnerability to hydrolytic cleavage seem to be the key structural features leading to the observed anion-dependent bacterial death. Interestingly, the antibacterial activity of imidazolium salts may be due to their amphiphilic structure, in which the hydrophilic cationic segments 2-dimethylimidazolium could have strong electrostatic interactions with the phosphate groups of DNA and hydrogen-bonding association of the anions, BF_4^-, and PF_6^-, with DNA bases.[43] Tetrafluoroborate salts are more bactericidal than hexafluorophosphate analogs because of $[BF_4^-]^-$ anions have a higher tendency to establish, on average, more hydrogen bonds with DNA bases than the $[PF_6]^-$ anion. Some discrepancies could be attributed to variations among microbe strains or to differences in the broth composition and inoculum density.

3.2. Antifungal activity

The in vitro antifungal activities of all the target compounds and Amphotericin B, as standard antifungal drug, were evaluated against two human pathogenic fungi, *A. flavus* and *C. albicans*. The results, ZOIs (cf. Fig. 2), demonstrate that all saldach-imidazolium salts and their Fe(III) complexes are inactive against *A. flavus* while exhibited moderate antifungal activity against *C. albicans* infection, and the ZOI values slightly increase as the concentration of the tested compound is raised from 2.5 to 20 mM. This limited or lack of fungicidal activity could be attributed to two possibilities: (i) the complex structure of fungal cell-wall, composed typically of chitin, 1,3-β- and 1,6-β-glucan, mannan, and proteins,[44] through which could neither diffuse nor decrease the rate of diffusion of tested compounds. (ii) Fungal fighting proceeds by much more complex mechanisms than bacterial conflict. *R,R*-Fe(III)^{i}Pr-saldach (**5d**), (MIC=75.21 mM) lower than the standard Amphotericin B, was identified as the most active against *C. albicans* and showed better *C. albicans* elimination capability by inhibiting the fungal growth even at 0.25 mM.

4. Conclusion

Broad-spectrum biocidal activity of newly fabricated chiral saldach-methylimidazolium ionic liquids (saldach-MIILs), *R,R*-H_2(R)$_2$saldach(2-MeIm$^+$X$^-$)$_2$, and their Fe(III) complexes have been investigated against common bacterial and fungal pathogens. Both the ZOIs assay and MIC values revealed that saldach-MIILs possessed significantly higher ability to inhibit the growth of *E. coli*<*B. subtilis*<*S. aureus* compared to Ampicillin antibiotic. The structure–activity (SA) comparison showed a strong relationship between antimicrobial efficacy and structure of the saldach backbone. Alkyl substituents on saldach backbone play a more important role in determining the biocidal properties of saldach-imidazolium architectures than the saldach-skeleton configuration. Substitution of the H-atom on saldach by an iso-propyl substituent dramatically decrease the minimal inhibitory concentrations, whereas, exchange of *meso*-dach with *R,R*-dach slightly decreases MIC. More importantly, anion metathesis has a smaller effect on antimicrobial activity of saldach-imidazolium salts. Eventually, refinements of the most active biocidal agent, [Fe^{III}Cl(^{iso}Pr-saldach(MeIm$^+$Cl$^-$)$_2$)] (**5d**) may serve as a platform towards the discovery of exceptionally active antimicrobial drugs.

5. Experimental

5.1. Material and methods

Elemental analyses for C, H, N, were performed with a Perkin–Elmer 263 elemental analyzer. FTIR spectra were recorded on a BRUKER Tensor-37 FTIR spectrophotometer in the range 400–4000 cm^{-1} as KBr disc or with an ATR (attenuated total reflection) unit (Platinum ATR-QL, diamond). UV–Vis spectra were measured at 25 °C in ethanol (10^{-5} mol/L) on a Shimadzu UV-2450 spectrophotometer using quartz cuvettes (1 cm). NMR-spectra were obtained with a Bruker Avance DRX200 (200 MHz for ^{1}H) or Bruker Avance DRX500 (125, 202, and 470 MHz for ^{13}C, ^{31}P, and ^{19}F, respectively) spectrometer with calibration to the residual proton solvent signal in DMSO-d_6 (^{1}H NMR: 2.52 ppm, ^{13}C NMR: 39.5 ppm), $CDCl_3$ (^{1}H NMR: 7.26 ppm, ^{13}C NMR: 77.16 ppm) against TMS (δ=0.00 ppm) for ^{1}H and ^{13}C, 85% phosphoric acid (δ=0.00 ppm) for

^{31}P and $CFCl_3$ (δ=0.00 ppm) for ^{19}F NMR. Multiplicities of the signals were specified s (singlet), d (doublet), t (triplet), q (quartet) or m (multiplet). The mass spectra of the synthesized saldach-bis(imidazolium) salts and their metal complexes were acquired in the linear mode for positive ions on a UHR-QTOF maXis 4G (Bruker Daltonics) and Bruker Ultraflex MALDI-TOF instrument equipped with a 337 nm nitrogen laser pulsing at a repetition rate of 10 Hz. The 2+ charge assignment of ions in HR-ESI-MS was confirmed by the m/z=0.5 difference between the isotope peaks (x, x+1, x+2). The MALDI matrix material (1,8-dihydroxy-9(10H)-anthracenone (dithranol, DIT, $^{12}C_{14}H_{10}O_3$, M=226.077 g/mol) was dissolved in chloroform at a concentration of 10 mg/mL. MALDI probes were prepared by mixing compound solution (1 mg/mL in CH_2Cl_2) with the matrix solution (1:10, v/v) in a 0.5 mL Eppendorf® micro tube. Finally 0.5 μL of this mixture was deposited on the sample plate, dried at room temperature and then analyzed. Peaks with chlorine showed the isotope ratio $^{35/37}$Cl=75.8:24.2. Manganese (^{55}Mn 54.938 Da, 100%) or iron (^{56}Fe 55.934 Da, 91.2%) are either isotope pure or with a predominant isotope (^{54}Fe 53.939, 5.8%; ^{57}Fe 56.935 Da, 2.1%). For the mass spectral assignment: Peaks are based on ^{12}C with 12.0000 Da, ^{35}Cl with 34.968 Da, ^{55}Mn 54.938 Da, ^{56}Fe 55.934. dithranol, DIT, $^{12}C_{14}H_{10}O_3$, M=226.077 g/mol. The molar conductances of 10^{-3} mol/L solution of various salts have been measured at ambient temperature with a digital conductivity meter (S30 SevenEasy™ conductivity, Mettler-Toledo Electronics, LLC, Polaris Parkway, Columbus). The overall accuracy of the conductance measurements was found to be ±0.2%.

Chemicals were obtained from the following suppliers and used without further purification: salicylaldehyde, 2-*iso*-propylphenol, (±)-*trans*-1,2-diaminocyclohexane (*rac*-*trans*-dach) and anhydrous $MgCl_2$ (Sigma–Aldrich), paraformaldehyde (Roth), 1,2-dimethylimidazole, 1-butylimidazole (Alfa Aesar), triethylamine (Et_3N), anhydrous $ZnCl_2$ (Grüssing GmbH), and $FeCl_3$ (Acros).

The preparation details of the key starting materials (*R*,*R*)-1,2-diaminocyclohexane (*R*,*R*-dach), 3-isopropylsalicylaldehyde (**1b**), 5-chloromethyl salicylaldehydes (**2a,b**), 3-(salicylaldehydes)-2-methylimidazolium chloride (**3a,b**), and anion metathesis products (**3c**–**f**) can be seen in Supplementary data.

5.2. General procedure for the preparation of *R*,*R*-R$_2$sal-dach(2-MeIm$^+$-X$^-$)$_2$ (4a–f)

A methanolic solution (10 mL) of (*R*,*R*)-1,2-diaminocyclohexane (*R*,*R*-dach) (0.23 g, 2.0 mmol) in a Schlenk tube, was added dropwise to a methanolic solution (20 mL) of salicylaldehyde-imidazolium salts (R)sal(MeIm$^+$-X$^-$) **3a**–**f** (4.0 mmol) into a 100 mL Schlenk flask under nitrogen atmosphere. The reaction mixture was stirred under N_2 at 60 °C for 3 h. Then the solvent was partially removed under reduced pressure, and the yellow products of **4a**–**f** were precipitated by the addition of ethyl acetate and kept in the refrigerator overnight. The solvent was decanted off and the obtained crude product was sonicated for 15 min in Et_2O (3×25 mL). Et_2O was also decanted off and the residual solid was washed intensively with a MeOH/Et_2O mixture (1:2) to remove unreacted materials and then re-dissolved in MeOH. EtOAc was added slowly (~15 min) to precipitate the products as pale yellow-dark orange solids, which were collected by filtration and dried under vacuum. Samples of the isolated solids were characterized as follows.

*5.2.1. N,N′-Bis-[5-((2-methylimidazolium chloride)methylene)-salicylidene)]-R,R-1,2-cyclohexanediamine dihydrate (**4a**).* Yellow-orange powder, (1.09 g, 87%). FTIR (KBr, cm^{-1}): 3345 (m, br, $\nu_{(N(1)-H)+\nu(O-H)}$), 3186 (w, br, $\nu_{asym(C-H)}$, CH, Im, and Ar), 3090 (m, br, $\nu_{sym(C-H)}$, Im, and Ar), 2295 (m, sh, $\nu_{(C=N)_{Im}}$), 1630 (vs, sh, $\nu_{(C=N)_{Azomethine}}$), 1558, 1475, 1387 (s, sh, $\nu_{(C=C_{Ar}+C-H_{bend})}$), 1274 (m, sh, $\nu_{(Ar-O)}$), 1160 (s, sh, $\nu_{(H-C=C+H-C=N)_{bend}}$, Im). ^{1}H NMR (200 MHz, $CDCl_3$) δ (ppm): 13.30 (2H, br, s, O**H**/N**H**), 9.48 (2H, s, 2Im–N*H*), 8.82 (2H, s, 2*H*–*C*=N), 7.85 (2H, d, J=1.8 Hz, 2N(1)CH*CH*–Im), 7.63 (2H, d, J=2.0 Hz, 2N(1)*CH*CH–Im), 7.52–7.28 (4H, m, 4Ar–**H**), 6.89–3.76 (2H, m, 2Ar–**H**), 5.30 (4H, s, 2 N(3)–*CH*$_2$–Ar), 3.91–3.77 (2H, m, 2 Cyhex–**H**), 3.38 (6H, s, 2 C(2)$_{Im}$–*CH*$_3$), 1.70–1.41 (8H, m, 8 Cyhex–**H**). ^{13}C NMR (125 MHz, $CDCl_3$) δ (ppm): 168.6, 160.2, 146.0, 132.9, 131.0, 124.9, 123.7, 122.4, 120.0, 118.7, 68.0, 51.3, 32.8, 24.1, and 12.8. MALDI-TOF MS, (m/z, amu): 659.4 [M·2H$_2$O+K]$^+$; HRMS (ESI): (m/z, amu): calcd for $C_{30}H_{36}N_6O_2\cdot 2H_2O$: 547.3835 [M·2H$_2$O–2Cl]$^+$; found: 547.3745. Anal. Calcd for $C_{30}H_{36}Cl_2N_6O_2\cdot 2H_2O$ (M=619.58): C, 58.16; H, 6.51; N, 13.56; Found: C, 57.84; H, 6.23; N, 13.51. Conductivity=284.1 μS/cm.

*5.2.2. N,N′-Bis-[5-((2-methylimidazolium hexafluorophosphate) methylene)-salicylidene)]-R,R-1,2-cyclohexanediamine (**4b**).* Faint Yellow powder, (1.17 g, 72%). FTIR (KBr, cm^{-1}): 3329 (m, br, $\nu_{(N(1)-H)+\nu(O-H)}$), 3191 (w, br, $\nu_{asym(C-H)}$, CH, Im, and Ar), 3068 (m, br, $\nu_{sym(C-H)}$, Im, and Ar), 2313 (m, sh, $\nu_{(C=N)_{Im}}$), 1637 (vs, sh, $\nu_{(C=N)_{Azomethine}}$), 1560, 1468, 1385 (s, sh, $\nu_{(C=C_{Ar}+C-H_{bend})}$), 1276 (m, sh, $\nu_{(Ar-O)}$), 1159 (s, sh, $\nu_{(H-C=C+H-C=N)_{bend}}$, Im), 840 (vs, sh, $\nu_{(PF_6^-)str}$). ^{1}H NMR (200 MHz, DMSO-d_6) δ (ppm): 13.33 (2H, d, J=2.3 Hz, O**H**/N**H**), 9.48 (2H, s, 2 Im–N*H*), 8.74 (2H, d, J=2.0 Hz, 2 *H*–*C*=N), 7.76 (2H, d, J=1.8 Hz, 2 N(1)CH*CH*–Im), 7.69 (2H, d, J=2.0 Hz, 2 N(1)*CH*CH–Im), 7.62 (2H, t, J_1=J_2=2.0 Hz, 2 Ar–**H**), 7.51 (2H, dd, J_1=2.5 Hz, J_2=5.3 Hz, 2 Ar–**H**), 6.92–6.81 (2H, m, 2 Ar–**H**), 5.51 (4H, s, 2 N(3)–*CH*$_2$–Ar), 3.90–3.78 (2H, m, 2 Cyhex–**H**), 3.36 (6H, s, 2 C(2)$_{Im}$–*CH*$_3$), 1.60–1.34 (m, 8H, 8 Cyhex–**H**). ^{13}C NMR (125 MHz, DMSO-d_6) δ (ppm): 168.4, 161.9, 142.9, 133.8, 132.5, 125.1, 124.5, 123.3, 120.0, 118.1, 65.4, 53.1, 33.8, 24.6, and 13.2. ^{31}P NMR (202 MHz, DMSO-d_6): −143.58 ppm (septet, $^2J_{PF}$=707.17 Hz). ^{19}F NMR (470 MHz, DMSO-d_6): −68.43 ppm (doublet, $^1J_{FP}$=705.65 Hz). MS (ESI$^+$) (m/z, amu): 657.5, [M–PF$_6^-$]; (ESI$^-$) (m/z, amu): 144.6. [PF$_6^-$]. Anal. Calcd for $C_{30}H_{36}F_{12}N_6O_2P_2$ (M=802.57): C, 44.90; H, 4.52; N, 10.47; Found: C, 55.11; H, 4.78; N, 10.23. Conductivity=259.3 μS/cm.

*5.2.3. N,N′-Bis-[5-((2-methylimidazolium tetrafluoroborate)methylene)-salicylidene)]-R,R-1,2-cyclohexanediamine monohydrate (**4c**).* Faint yellow powder, (0.92 g, 65%). FTIR (KBr, cm^{-1}): 3323 (m, br, $\nu_{(N(1)-H)+\nu(O-H)}$), 3177 (w, br, $\nu_{asym(C-H)}$, CH, Im, and Ar), 3042 (m, br, $\nu_{sym(C-H)}$, Im, and Ar), 2298 (m, sh, $\nu_{(C=N)_{Im}}$), 1636 (vs, sh, $\nu_{(C=N)_{Azomethine}}$), 1580, 1472, 1387 (s, sh, $\nu_{(C=C_{Ar}+C-H_{bend})}$), 1273 (m, sh, $\nu_{(Ar-O)}$), 1147 (s, sh, $\nu_{(H-C=C+H-C=N)_{bend}}$, Im), 1059 (vs, sh, $\nu_{(BF_4^-)str}$). ^{1}H NMR (200 MHz, DMSO-d_6) δ (ppm): 13.59 (2H, d, J=3.2 Hz, O**H**/N**H**), 9.13 (2H, s, 2 Im–N*H*), 8.77 (2H, d, J=2.0 Hz, 2*H*–*C*=N), 7.73 (2H, d, J=1.6 Hz, 2 N(1)CH*CH*–Im), 7.69 (2H, d, J=1.5 Hz, 2 N(1)*CH*CH–Im), 7.54 (2H, t, J_1=J_2=2.1 Hz, 2 Ar–**H**), 7.43 (2H, dd, J_1=2.2 Hz, J_2=6.0 Hz, 2 Ar–**H**), 6.92 (2H, d, J=7.8 Hz, 2 Ar–**H**), 5.36 (4H, s, 2 N(3)–*CH*$_2$–Ar), 3.94–3.81 (2H, m, 2 Cyhex–**H**), 3.41 (6H, s, 2 C(2)$_{Im}$–*CH*$_3$), 1.84–1.67 (4H, m, 4 Cyhex–**H**), 1.56–1.41 (4H, m, 4 Cyhex–**H**). ^{13}C NMR (125 MHz, DMSO-d_6) δ (ppm): 168.3, 161.3, 142.0, 132.9, 132.0, 124.7, 124.0, 123.1, 119.4, 117.3, 63.8, 52.7, 34.2, 24.0, and 13.2. B^{19}F NMR (470 MHz, DMSO-d_6): −146.81 ppm (singlet). MS (ESI$^+$) (m/z, amu): 599.2, [M–BF$_4^-$]; (ESI$^-$) (m/z, amu): 87.0 [BF$_4^-$]. Anal. Calcd for $C_{30}H_{36}B_2F_8N_6O_2$ (M=686.26): C, 52.51; H, 5.29; N, 12.25; Found: C, 55.63; H, 5.71; N, 12.00. Conductivity=267.1 μS/cm.

*5.2.4. N,N′-Bis-[3-iso-propyl-5-((2-methylimidazolium chloride) methylene)-salicylidene)]-R,R-1,2-cyclohexanediamine (**4d**).* Yellow-orange powder, (1.12 g, 83%). FTIR (KBr, cm^{-1}): 3334 (m, br, $\nu_{(N(1)-H)+\nu(O-H)}$), 3129 (m, sh, $\nu_{asym(C-H)}$, Im, and Ar), 3074 (m, sh, $\nu_{sym(C-H)}$, Im, and Ar), 2313 (m, sh, $\nu_{(C=N)_{Im}}$), 1629 (vs, sh, $\nu_{(C=N)_{Azomethine}}$), 1532, 1461, 1388 (s, sh, $\nu_{(C=C_{Ar}+C-H_{bend})}$), 1271 (s, sh, $\nu_{(Ar-O)}$), 1163 (s, sh, $\nu_{(H-C=C+H-C=N)_{bend}}$, Im). ^{1}H NMR (200 MHz, $CDCl_3$) δ (ppm): 13.95 (s,

2H, O**H**/N**H**), 9.33 (2H, s, 2 Im–N**H**), 8.68 (2H, s, 2*H*–*C*=N), 7.79 (2H, d, *J*=2.0 Hz, 2 N(1)CHC*H*–Im), 7.73 (d, *J*=1.98 Hz, 2H, 2 N(1) *CH*CH–Im), 7.41 (2H, d, *J*=1.52 Hz, 2 Ar–**H**), 7.25 (2H, d, *J*=1.8 Hz, 2 Ar–**H**), 5.37 (4H, s, 2 N(3)–CH_2–Ar), 3.77 (6H, s, 2 $C(2)_{Im}$–CH_3), 3.40–3.29 (2H, m, 2 Cyhex–**H**), 3.22–312 (2H, m, 2 $CH(CH_3)_2$), 3.03 (6H, s, 2 $C(2)_{Im}$–CH_3), 1.81–1.67 (4H, m, 4 Cyhex–**H**), 1.52–1.38 (4H, m, 4 Cyhex–**H**), 1.16 (12H, d, *J*=7.9 Hz, 2 $CH(CH_3)_2$). ^{13}C NMR (125 MHz, $CDCl_3$) δ (ppm): 171.3, 160.0, 143.8, 137.7, 131.9, 124.4, 123.0, 121.2, 117.9, 68.7, 52.1, 34.8, 32.9, 29.4, 24.2, and 10.7. (ESI$^+$) (*m*/*z*, amu): 657.5, [M–Cl$^-$]; (ESI$^-$) (*m*/*z*, amu): 35.4. [Cl$^-$]. Anal. Calcd for $C_{36}H_{48}Cl_2N_6O_2$ (*M*=666.32): C, 64.76; H, 7.25; N, 12.59; Found: C, 64.78; H, 7.47; N, 12.34. Conductivity=106.9 μS/cm.

*5.2.5. N,N′-Bis-[3-iso-propyl-5-((2-methylimidazolium hexafluorophosphate)methylene)-salicylidene)]-R,R-1,2-cyclohexanediamine monohydrate (**4e**).* Canary yellow powder, (1.26 g, 69%). FTIR (KBr, cm^{-1}): 3332 (m, br, $\nu_{(N(1)-H)}$+$\nu_{(O-H)}$), 3163 (m, sh, $\nu_{asym(C-H)}$, Im, and Ar), 3054 (m, sh, $\nu_{sym(C-H)}$, Im, and Ar), 2303 (m, sh, $\nu_{(C=N)_{Im}}$), 1633 (vs, sh, $\nu_{(C=N)_{Azomethine}}$, 1537, 1460, 1391 (s, sh, $\nu_{(C=C_{Ar}+C-H_{bend})}$), 1273 (s, sh, $\nu_{(Ar-O)}$), 1159 (s, sh, $\nu_{(H-C=C+H-C=N)_{bend}}$, Im), 837 (vs, sh, $\nu_{(PF_6^-)str}$).^{1}H NMR (200 MHz, DMSO-d_6) δ (ppm): 13.99 (2H, s, O**H**/N**H**), 9.41 (2H, s, 2 Im–N**H**), 8.53 (2H, s, 2*H*–*C*=N), 7.70 (2H, d, *J*=2.0 Hz, 2 N(1)CHC*H*–Im), 7.64 (2H, d, *J*=2.0 Hz, 2 N(1)*CH*CH–Im), 7.32 (2H, d, *J*=2.0 Hz, 2 Ar–**H**), 7.21 (2H, d, *J*=2.2 Hz, 2 Ar–**H**), 5.48 (4H, s, 2 N(3)–CH_2–Ar), 3.50 (2H, s, br, 2 Cyhex–**H**), 3.23–3.07 (2H, m, 2 $CH(CH_3)_2$), 2.68 (6H, s, 2 $C(2)_{Im}$–CH_3), 1.83–1.68 (4H, m, 4 Cyhex–**H**), 1.53–1.39 (4H, m, 4 Cyhex–**H**), 1.33 (12H, dd, J_1=1.6 Hz, J_2=6.9 Hz, 2 $CH(CH_3)_2$). ^{13}C NMR (125 MHz, DMSO-d_6) δ (ppm): 172.0, 160.1, 144.7, 137.7, 129.9, 123.9, 122.9, 121.2, 118.5, 71.2, 50.7, 32.9, 29.4, 26.7, 24.1, and 9.8. ^{31}P NMR (202 MHz, DMSO-d_6): −143.21 ppm (septet, $^2J_{PF}$=712.03 Hz). ^{19}F NMR (470 MHz, DMSO-d_6): −70.56 ppm (doublet, $^1J_{FP}$=716.71 Hz). MS (ESI$^+$) (*m*/*z*, amu): 742.2, [M–PF$_6^-$]; (ESI$^-$) (*m*/*z*, amu): 144.5. [PF$_6^-$]. Anal. Calcd for $C_{36}H_{48}F_{12}N_6O_2P_2\cdot H_2O$ (*M*=904.75): C, 47.79; H, 5.57; N, 9.29; Found: C, 47.93; H, 5.75; N, 9.20. Conductivity=71.5 μS/cm.

*5.2.6. N,N′-Bis-[3-iso-propyl-5-((2-methylimidazolium tetrafluoroborate)methylene)-salicylidene)]-R,R-1,2-cyclohexanediamine monohydrate (**4f**).* Pale yellow powder, (1.06 g, 67%). FTIR (KBr, cm^{-1}): 3339 (m, br, $\nu_{(N(1)-H)}$+$\nu_{(O-H)}$), 3185 (m, sh, $\nu_{asym(C-H)}$, Im, and Ar), 3151 (m, sh, $\nu_{sym(C-H)}$, Im, and Ar), 2291 (m, sh, $\nu_{(C=N)_{Im}}$), 1631 (vs, sh, $\nu_{(C=N)_{Azomethine}}$, 1537, 1465, 1389 (s, sh, $\nu_{(C=C_{Ar}+C-H_{bend})}$), 1274 (s, sh, $\nu_{(Ar-O)}$), 1159 (s, sh, $\nu_{(H-C=C+H-C=N)_{bend}}$, Im), 1061 (vs, sh, $\nu_{(BF_4^-)str}$).^{1}H NMR (200 MHz, DMSO-d_6) δ (ppm): 14.03 (2H, s, O**H**/N**H**), 9.43 (2H, s, 2 Im–N**H**), 8.55 (2H, s, 2 *H*–*C*=N), 7.68 (2H, d, *J*=2.1 Hz, 2 N(1) CHC*H*–Im), 7.61 (2H, d, *J*=2.0 Hz, 2 N(1)*CH*CH–Im), 7.38 (2H, d, *J*=2.0 Hz, 2 Ar–**H**), 7.26 (2H, d, *J*=2.0 Hz, 2 Ar–**H**), 5.39 (4H, s, 2 N(3)–CH_2–Ar), 3.53 (2H, s, br, 2 Cyhex–**H**), 3.22–3.12 (2H, m, 2 $CH(CH_3)_2$), 2.66 (6H, s, 2$C(2)_{Im}$–CH_3), 1.84–1.68 (4H, m, 4 Cyhex–**H**), 1.49–1.34 (4H, m, 4 Cyhex–**H**), 1.17 (12H, dd, J_2=7.0 Hz, J_1=1.4 Hz, 2 $CH(CH_3)_2$). ^{13}C NMR (125 MHz, DMSO-d_6) δ (ppm): 173.3, 159.8, 144.7, 136.5, 129.4, 124.5, 122.9, 121.2, 118.1, 71.4, 50.6, 33.1, 26.4, 24.4, 22.7, and 9.8. ^{19}F NMR (470 MHz, DMSO-d_6): −148.68 ppm (singlet). MS (ESI$^+$) (*m*/*z*, amu): 683.4, [M–BF$_4^-$]; (ESI$^-$) (*m*/*z*, amu): 87.0 [BF$_4^-$]. Anal. Calcd for $C_{36}H_{48}B_2F_8N_6O_2$ H_2O (*M*=788.40): C, 54.84; H, 6.39; N, 10.66; Found: C, 55.06; H, 6.65; N, 10.28. Conductivity=78.6 μS/cm.

5.3. General procedure for the preparation of chloridometallosaldach-bis-imidazolium complexes [Fe(III)Cl{$(R)_2$ saldach(MeIm$^+$-X$^-$)$_2$}] (5a–f)

A yellow solution of the saldach-bis(imidazolium) salts $H_2(R)_2$saldach(MeIm$^+$X$^-$)$_2$, **4a**–**f**, (0.9 mmol) in ethanol (10 mL) was degassed for 15 min. An ethanolic solution (5 mL) of $FeCl_3$ (1.77 g, 1.1 mmol) was then added with the yellow solution turning dark reddish-brown immediately, and the reaction mixture was refluxed for 2 h under N_2. Then, the solution was concentrated and the residue was kept in a refrigerator overnight. The precipitated solid was filtered off and washed with cold ethanol (2×3 mL) and diethyl ether (3×3 mL) to yield [Fe(III)Cl{$(R)_2$saldach(MeIm$^+$X$^-$)$_2$}] (**5a**–**f**).

*5.3.1. [Fe^{III}Cl(saldach(MeIm$^+$Cl$^-$)$_2$)]·H_2O (**5a**·H_2O).* Reddish-brown powder (0.53 g, 86% based on Fe). FTIR (KBr, cm^{-1}): 3441 (m, br, $\nu_{(O-H)}$, lattice water), 3344 (m, br, $\nu_{(N(1)-H)}$), 1617 (vs, sh, $\nu_{(C=N)}$), 1281 (m, sh, $\nu_{(Ar-O)}$), 817, 761, 591, 547, 471, 432. MS MALDI-TOF (*m*/*z*, amu): 692.2 (9%, [M·H_2O+H]$^+$), 507.1 (17%, [Fe(DIT)$_2$–H$^+$]$^+$, 227.0 (100%, [DIT+H$^+$]$^+$). Anal. Calcd for $C_{30}H_{34}FeN_6O_2\cdot H_2O$ (*M*=690.85): C, 52.16; H, 5.25; N, 12.16; Found: C, 52.24; H, 5.32; N, 11.79. Conductivity=349.0 μS/cm.

*5.3.2. [Fe^{III}Cl(saldach(MeIm$^+$PF$_6^-$)$_2$)]·$2H_2O$ (**5b**·$2H_2O$).* Brown powder (0.58 g, 69% based on Fe). FTIR (KBr, cm^{-1}): 3516 (m, br, $\nu_{(O-H)}$, lattice water), 3283 (m, br, $\nu_{(N(1)-H)}$), 1620 (vs, sh, $\nu_{(C=N)}$), 1283 (m, sh, $\nu_{(Ar-O)}$), 841 (vs, sh, $\nu_{(PF_6^-)str}$), 760, 587, 542, 468, 429. MS (ESI$^+$) (*m*/*z*, amu): 746.5 [M–PF$_6^-$]; (ESI$^-$) (*m*/*z*, amu): 144.6. [PF$_6^-$]. Anal. Calcd for $C_{30}H_{34}FeN_6O_2\cdot 2H_2O$ (*M*=927.89): C, 38.83; H, 4.13; N, 9.06; Found: C, 39.11; H, 4.19; N, 8.94. Conductivity=306.4 μS/cm.

*5.3.3. [Fe^{III}Cl(saldach(MeIm$^+$BF$_4^-$)$_2$)]·H_2O (**5c**·H_2O).* Faint brown powder (0.51 g, 71% based on Fe). FTIR (KBr, cm^{-1}): 3498 (m, br, $\nu_{(O-H)}$, lattice water), 3285 (m, br, $\nu_{(N(1)-H)}$, 1619 (vs, sh, $\nu_{(C=N)}$), 1282 (m, sh, $\nu_{(Ar-O)}$), 1060 (vs, sh, $\nu_{(BF_4^-)str}$), 759, 579, 539, 467, 430. MS (ESI$^+$) (*m*/*z*, amu): 688.1 [M–BF$_4^-$]$^+$; (ESI$^-$) (*m*/*z*, amu): 87.1 [BF$_4$]$^-$. Anal. Calcd for $C_{30}H_{34}B_2ClF_8FeN_6O_2\cdot H_2O$ (*M*=793.55): C, 45.41; H, 4.57; N, 10.59; Found: C, 39.11; H, 4.19; N, 8.94. Conductivity=314.3 μS/cm.

*5.3.4. [Fe^{III}Cl(iso-Pr-saldach(MeIm$^+$Cl$^-$)$_2$)]·H_2O (**5d**·H_2O).* Brick-red powder (0.51 g, 73%). FTIR (KBr, cm^{-1}): 3498 (m, br, $\nu_{(O-H)}$, lattice water), 3287 (m, sh, $\nu_{asym(C-H)}$, Im, and Ar), 1613 (vs, sh, $\nu_{(C=N)}$), 1282 (s, sh, $\nu_{(Ar-O)}$), 834, 764, 678, 570, 545, 498, 467. MS MALDI-TOF, (*m*/*z*, amu): 747.3 (12%, [M+DIT–MeImH$^+$Cl$^-$–MeIm–Cl$^-$]$^+$), 521.2 (79%, [M–2 MeIm–2 Cl$^-$]$^{2+}$), 507.1 (23%, [Fe(DIT)$_2$–H$^+$]$^+$, 226.9 (100%, [DIT+H$^+$]$^+$). Anal. Calcd for $C_{36}H_{46}Cl_3FeN_6O_2\cdot H_2O$ (*M*=775.01): C, 55.79; H, 6.24; N, 10.84; Found: C, 56.00; H, 6.41; N, 10.65. Conductivity=94.7 μS/cm.

*5.3.5. [Fe^{III}Cl(iso-Pr-saldach(MeIm$^+$PF$_6^-$)$_2$)]·~$2H_2O$ (**5e**·~$2H_2O$).* Brown powder (0.59 g, 65%). FTIR (KBr, cm^{-1}): 3430 (m, br, $\nu_{(O-H)}$, lattice water), 3283 (m, br, $\nu_{(N(1)-H)}$), 1617 (vs, sh, $\nu_{(C=N)}$), 1287 (s, sh, $\nu_{(Ar-O)}$), 842 (vs, sh, $\nu_{(PF_6^-)str}$), 780, 763, 680, 572, 557, 471. MS MALDI-TOF, (*m*/*z*, amu): 746.3 (<5%, [M+DIT–MeImH$^+$PF$_6^-$–MeIm–PF$_6^-$]$^+$), 521.2 (40%, [M–2 Me_2Im–2 PF$_6^-$]$^{2+}$), 507.1 (20%, [Fe(DIT)$_2$–H$^+$]$^+$, 227.0 (100%, [DIT+H$^+$]$^+$). Anal. Calcd for $C_{36}H_{46}ClF_{12}FeN_6O_2P_2\cdot$~$2H_2O$ (*M*=1011.22): C, 42.72; H, 4.98; N, 8.30; Found: C, 42.55; H, 5.13; N, 8.16. Conductivity=80.1 μS/cm.

*5.3.6. [Fe^{III}Cl(iso-Pr-saldach(MeIm$^+$BF$_4^-$)$_2$)]·H_2O (**5f**·H_2O).* Dark-red powder (0.53 g, 67%). FTIR (KBr, cm^{-1}): 3442 (m, br, $\nu_{(O-H)}$, lattice water), 3289 (m, br, $\nu_{(N(1)-H)}$), 1622 (vs, sh, $\nu_{(C=N)}$), 1284 (s, sh, $\nu_{(Ar-O)}$), 1060 (vs, sh, $\nu_{(BF_4^-)str}$), 834, 768, 678, 573, 550, 497, 465, 443. MS MALDI-TOF, (*m*/*z*, amu): 521.2 (15%, [M–2 Me_2Im–2 BF$_4^-$]$^{2+}$), 507.1 (5%, [Fe(DIT)$_2$–H$^+$]$^+$, 227.0 (100%, [DIT+H$^+$]$^+$). Anal. Calcd for $C_{36}H_{46}B_2ClF_8FeN_6O_2\cdot H_2O$ (*M*=877.29): C, 49.26; H, 5.51; N, 9.57; Found: C, 49.54; H, 5.78; N, 9.33. Conductivity=86.9 μS/cm.

5.4. Antibacterial survey

5.4.1. Reagents. Dimethylsulphoxide (DMSO) and Ampicillin antibiotic ($C_{16}H_{19}N_3O_4S$, 349.41 g/mol) and Antifungal drug

(Amphotericin B, $C_{47}H_{73}NO_{17}$) were obtained from Sigma Chemical Co. (St. Louis, MO, USA).

5.4.2. Microbial cultures. Multi-drug resistant (MDR) strains used in this study from National Organization for Drug Control and Research (NODCAR), Cairo, Egypt. The different strains are *Staphylococcus aureus* (*S. aureus*, ATCC-25923), Bacillus subtilis (*B. subtilis*, Re-cultured), and *Streptococcus pneumoniae* as representatives for the Gram-positive bacteria and *Escherichia coli* (*E. coli*, ATCC-25922) and Pseudomonas aeruginosa (*P. aeruginosa*, ATCC-27853) as the most important Gram-negative pathogenic bacteria. Antifungal species are Aspergillus flavus (*A. flavus*) and Candida albicans (*C. albicans*, NCIM No. 3100). Stock cultures grown aerobically on nutrient broth (NB) agar slants (Hi-Media) at 37 °C were maintained at 4 °C. Pre-cultures containing 10^5 CFU/ml, grown aerobically in Mueller Hinton (MH) liquid medium (Hi-Media) at 37 °C for 5 h, were used as inoculum for all experiments.

5.4.3. Antimicrobial susceptibility. Antimicrobial susceptibility of the bacterial/fungal strains was carried out by agar well diffusion method[45] toward the target compounds as well as standard drugs, Ampicillin and Amphotericin B. The diameter of the zones of inhibition (ZOI, mm) was measured accurately as indicative of antimicrobial activity.

5.4.3.1. Determination of MIC and MBC. As a parameter of the antimicrobial efficacy, the minimal inhibitory concentration (MIC) and minimal bactericidal concentration (MBC) of new compounds against Gram-positive, Gram-negative, and fungal isolates were determined using the macro-dilution broth susceptibility test. Freshly prepared MH broth was used as diluents in the macro-dilution method. A serial dilution of each target compound was prepared within a desired range (0.25 mM–20.00 mM). One milliliter of the Stock cultures was then inoculated and tubes were incubated at 37 °C for 24 h, control tubes without any addition were assayed simultaneously. MIC was examined visually, by checking the turbidity of the tubes. Furthermore the tubes having lesser concentration than MIC level were inoculated on MHA plate for MBC determination.

Acknowledgements

This work was in part supported by DFG grant Ja466/24-1 (initiation of bilateral cooperation RFME-CJ) and DAAD (WAP, A/12/05553).

Supplementary data

Supplementary data (experimental, spectral, and biological data) associated with this article are available with the article through the journal Web site, at http://dx.doi.org/10.1016/j.tet.2014.08.034.

References and notes

1. Tanitame, A.; Oyamada, Y.; Ofuji, K.; Fujimoto, M.; Suzuki, K.; Ueda, T.; Terauchi, H.; Kawasaki, M.; Nagai, K.; Yamagishi, J. *Bioorg. Med. Chem.* **2004**, *12*, 5515–5524.
2. Chu, D. T.; Plattner, J. J.; Katz, L. *J. Med. Chem.* **1996**, *39*, 3853–3874.
3. Ballell, L.; Field, R. A.; Duncan, K.; Young, R. J. *Antimicrob. Agents Chemother.* **2005**, *49*, 2153–2163.
4. Barrett, J. F.; Hoch, J. A. *Antimicrob. Agents Chemother.* **1998**, *42*, 1529–1536.
5. Miyamoto, T.; Matsumoto, J.; Chiba, K.; Egawa, H.; Shibamori, K.; Minamida, A.; Nishimura, Y.; Okada, H.; Kataoka, M.; Fujita, M.; Hirose, T.; Nakano, J. *J. Med. Chem.* **1990**, *33*, 1645–1656.
6. Nakada, N.; Shimada, H.; Hirata, T.; Aoki, Y.; Kamiyama, T.; Watanabe, J.; Arisawa, M. *Antimicrob. Agents Chemother.* **1993**, *37*, 2656–2661.
7. Correia, I.; Pessoa, J. C.; Duarte, M. T.; Minas da Piedade, M. F.; Jackush, T.; Kiss, T.; Castro, M. M. C. A.; Geraldes, C. F. G. C.; Avecilla, F. *Eur. J. Inorg. Chem.* **2005**, 732–744.
8. (a) Barton, D.; Ollis, W. D. *Comprehensive Organic Chemistry*; Pergamon: Oxford, 1979, Vol. 2; (b) Layer, R. W. *Chem. Rev.* **1963**, *63*, 489–510.
9. Tanaka, H.; Agar, A.; Yavuz, M. *J. Mol. Model.* **2010**, *16*, 577–587.
10. Katsuki, T. *Coord. Chem. Rev.* **1995**, *140*, 189–214.
11. (a) Becker, R. S.; Lenoble, C.; Zein, A. *J. Phys. Chem.* **1987**, *91*, 3509–3517; (b) Seliger, J.; Zagar, V.; Blinc, R.; Hadjoudis, E.; Milia, F. *Chem. Phys.* **1990**, *142*, 237–244; (c) Tezer, N.; Karakus, N. *J. Mol. Model.* **2009**, *15*, 223–232.
12. (a) Asiri, A. M.; Badahdah, K. O. *Molecules* **2007**, *12*, 1796–1804; (b) Novak, P.; Škare, D.; Sekušak, S.; Vikić-Topić, D. *Croat. Chem. Acta* **2000**, *73*, 1153–1170; (c) Tanak, H.; Alpaslan, Y. B.; Yavuz, M.; Ağar, E.; Erşahin, F.; Büyükgüngör, O. *Acta Crystallogr.* **2009**, *E65*, o1572.
13. (a) Bhattacharya, S.; Mandal, S. S. *Chem. Commun.* **1996**, 1515–1516; (b) Burrows, C. J.; Hickerson, R. P.; Muller, J. G.; Felden, B.; Rokita, S. E. *Biophys. J.* **1999**, *76* A5–a5; (c) Routier, S.; Bernier, J. L.; Waring, M. J.; Colson, P.; Houssier, C.; Bailly, C. *J. Org. Chem.* **1996**, *61*, 2326–2331; (d) Shrivastava, H. Y.; Devaraj, S. N.; Nair, B. U. *J. Inorg. Biochem* **2004**, *98*, 387–392.
14. Rokita, S. E.; Burrows, C. J. *Salen-metal Complexes, Small Molecule DNA and RNA Binders*; Wiley-VCH, 2003, Vol. 1.
15. Muller, J. G.; Kayser, L. A.; Paikoff, S. J.; Duarte, V.; Tang, N.; Perez, R. J.; Rokita, S. E.; Burrows, C. J. *Coord. Chem. Rev.* **1999**, *185–186*, 761–774.
16. (a) Irisawa, M.; Takeda, N.; Komiyama, M. *J. Chem. Soc., Chem. Commun.* **1995**, 1221–1222; (b) Komiyama, M.; Takeda, N.; Shigekawa, H. *Chem. Commun.* **1999**, 1443–1452; (c) Prema, D.; Wiznycia, A. V.; Scott, B. M.; Hilborn, J.; Desper, J.; Levy, C. J. *Dalt. Trans.* **2007**, *42*, 4788–4796.
17. (a) Pernak, J.; Goc, I.; Mirska, I. *Green. Chem.* **2004**, *6*, 323–329; (b) Demberelnyamb, D.; Kim, K. S.; Choi, S.; Park, S. Y.; Lee, H.; Kim, C. J.; Yoo, I. D. *Bioorg. Med. Chem.* **2004**, *12*, 853–857; (c) Pernak, J.; Sobaszkiewicz, K.; Mirska, I. *Green. Chem.* **2003**, *5*, 52–56; (d) Pernak, J.; Sobaszkiewicz, K.; Joanna, F.-F. *Chem. Eur. J.* **2004**, *10*, 3479–3485.
18. Stock, F.; Hoffman, J.; Ranke, J.; Ondruschka, B.; Jastorff, B. *Green. Chem.* **2004**, *6*, 286–290.
19. Hosseinzadeh, F.; Mahkam, M.; Galehassadi, M. *Des. Monomers Polym.* **2012**, *15*, 379–388.
20. Malhotra, S. V.; Kumar, V. *Bioorg. Med. Chem. Lett.* **2010**, *20*, 581–585.
21. Carson, L.; Chau, P. K.; Earle, M. J.; Gilea, M. A.; Gilmore, B. F.; Gorman, S. P.; McCann, M. T.; Seddon, K. R. *Green. Chem.* **2009**, *11*, 492–497.
22. (a) Bennani, Y. L.; Hanessian, S. *Chem. Rev.* **1997**, *97*, 3161–3196; (b) Borisova, N. E.; Reshetova, M. D.; Ustynyuk, Y. A. *Chem. Rev.* **2007**, *107*, 46–79.
23. (a) Jongwoo, P.; Kai, L.; Khalil, A.; Sukwon, H. *J. Am. Chem. Soc.* **2008**, *130*, 16484–16485; (b) Rong, T.; Donghong, Y.; Ningya, Y.; Haihong, Z.; Dulin, Y. J. *Catal* **2009**, *263*, 284–291; (c) Song, F.-J.; Wang, C.; Falkowski, J.; Ma, L.; Lin, W. *J. Am. Chem. Soc.* **2010**, *132*, 15390–15398.
24. (a) Chang, T.; Jin, L.; Jing, H. *ChemCatChem* **2009**, *1*, 379–383; (b) Naik, P. U.; McManus, G. J.; Zaworotko, M. J.; Singer, R. D. *Dalt. Trans.* **2008**, 4834–4836; (c) Kureshy, R. I.; Prathap, K. J.; Roy, T.; Maity, N. C.; Khan, N.; Abdi, S. H.; Bajaj, H. *Adv. Synth. Catal.* **2010**, *352*, 3053–3060.
25. (a) Mahmoud, R. F.; Janiak, C. *Acta Crystallogr. E* **2009**, *65*, m909–m910; (b) Elshaarawy, R. F. M.; Janiak, C. Z. *Naturforsch* **2011**, *66b*, 1202–1208; (c) Elshaarawy, R. F. M.; Lan, Y.; Janiak, C. *Inorg. Chim. Acta* **2013**, *401*, 85–94.
26. (a) Refat, M. S.; El-Deen, I. M.; Elshaarawy, R. F. *Russ. J. Gen. Chem.* **2014**, *84*, 593–601; (b) Wisser, B.; Janiak, C. Z. *Anorg. Allg. Chem.* **2007**, *633*, 1796–1800; (c) Ibrahim, H. K.; Eltamany, E.; Elshaarawy, R. F. M.; Mohy-Eldeen, I. *Maced. J. Chem. Chem. Eng.* **2008**, *27*, 65–79.
27. (a) Elshaarawy, R. F. M.; Janiak, C. *Eur. J. Med. Chem.* **2014**, *75*, 31–42; (b) Elshaarawy, R. F. M.; Kheiralla, Z. H.; Rushdy, A. A.; Janiak, C. *Inorg. Chim. Acta* **2014**, *421*, 110–122.
28. Campbell, J. L. E.; Johnson, K. E.; Torkelson, J. R. *Inorg. Chem.* **1994**, *33*, 3340–3345.
29. Azam, M.; Hussain, Z.; Warad, I.; Al-Resayes, S. I.; Khan, M. S.; Shakir, M.; Trzesowska-Kruszynskae, A.; Kruszynski, R. *Dalt. Trans.* **2012**, *41*, 10854–10864.
30. Mauryaa, M. R.; Chandrakar, A. K.; Chand, S. *J. Mol. Cat. A* **2007**, *270*, 225–235.
31. (a) Webster, F. X.; Silverstein, R. M. *Spectrophotometer Identification of Organic Compounds*, 6th ed.; John Wiley: New York, 1992; p 87; (b) Pouralimardan, O.; Chamayou, A.-C.; Janiak, C.; Monfared, H. H. *Inorg. Chim. Acta* **2007**, *360*, 1599–1608.
32. (a) Nakomoto, K. *Infrared and Raman Spectroscopy of Inorganic and Coordination Compounds*, 3rd ed.; Wiley Interscience: New York, 1978; (b) Guojin, X.; Saili, W.; Yingguo, F.; Libo, Z.; Yuhai, T.; Yuansuo, Z. *Chin. J. Catal.* **2012**, *33*, 473–477.
33. (a) Nazir, H.; Yildiz, M.; Yilmaz, H.; Tahir, M.; Ülku, D. *J. Mol. Struct.* **2000**, *524*, 241–250; (b) Odababaşoğlu, M.; Özkanza, R.; Aykan, F. Z.; Lonecke, P. *J. Mol. Struct.* **2007**, *840*, 71–89; (c) Drašković, B. M.; Bogdanović, G. A.; Neelakantan, M. A.; Chamayou, A.-C.; Thalamuthu, S.; Avadhut, Y. S.; Schmedt auf der Günne, J.; Banerjee, S.; Janiak, C. *Cryst. Growth Des.* **2010**, *10*, 1665–1676.
34. Claramunt, R. M.; Lopez, C.; Santa María, M. D.; Sanz, D. *J. Prog. Nucl. Magn. Reson. Spectrosc.* **2006**, *49*, 169–206.
35. Alarcon, S. H.; Olivieri, A. C.; Gonzalez-Sierra, M. *J. Chem. Soc. Perkin Trans.* **1994**, 1067–1070.
36. (a) Cort, A. D.; Gasparrini, F.; Lunazzi, L.; Mandolini, L.; Mazzanti, A.; Pasquini, C.; Pierini, M.; Rompietti, R.; Schiaffino, L. J. *Org. Chem.* **2005**, *70*, 8877–8883; (b) Boghaei, D. M.; Mohebi, S. J. *Chem. Res. Synop.* **2002**, 72–75.

37. Alarcón, S. H.; Olivieri, A. C.; Sanz, D.; Claramunt, R. M.; Elguero, J. *J. Mol. Struct.* **2004**, *705*, 1–9.
38. (a) Bosnich, B. *J. Am. Chem. Soc.* **1968**, *90*, 627–632; (b) Di Bella, S.; Fragala, I.; Ledoux, I.; Diaz-Garcia, M. A.; Marks, T. J. *J. Am. Chem. Soc.* **1997**, *119*, 9550–9557.
39. Boucher, L. J.; Farrell, M. *J. Inorg. Nucl. Chem.* **1973**, *35*, 3731–3738.
40. Gaber, B. P.; Miskowski, V.; Spiro, T. G. *J. Am. Chem. Soc.* **1974**, *96*, 6868–6873.
41. Dickson, J.; Koohmaraie, M. *Appl. Environ. Microbiol.* **1989**, *55*, 832–836.
42. Hille, A.; Gust, R. *Arch. Pharm. Chem. Life Sci.* **2009**, *342*, 625–631.
43. Cardoso, L.; Micaelo, N. M. *ChemPhysChem* **2011**, *12*, 275–277.
44. Hector, R. F. *Clin. Microbiol. Rev.* **1993**, *6*, 1–21.
45. Perez, C.; Bazerque, P. M. *Acta Biol. Med. Exp.* **1990**, *15*, 113–115.